Journal of Sound and Vibration (2001) **239**(3), 445–466
doi:10.1006/jsvi.2000.3172, available online at http://www.idealibrary.com on IDEAL®

MODELLING THE DYNAMIC BEHAVIOUR OF A SUPERCRITICAL ROTOR ON A FLEXIBLE FOUNDATION USING THE MECHANICAL IMPEDANCE TECHNIQUE

P. BONELLO AND M. J. BRENNAN

Institute of Sound and Vibration Research, University of Southampton, Highfield, Southampton, SO17 1BJ, England. E-mail: ppb@isvr.soton.ac.uk

(*Received* 19 *April* 1999, *and in final form* 5 *June* 2000)

Rotating machinery in industry is usually placed on foundation structures that are flexible over the operational speed range and thus influence the dynamics of the coupled system. The mechanical impedance method offers a computationally efficient means of developing simple, but sufficiently accurate analytical linear models of such systems, for most practical purposes. The technique facilitates a modelling approach where a mixture of theoretical and experimental models can be incorporated into a model of the complete system. This is particularly useful when modifying existing machinery, where, for example, it may be easier and cheaper to measure the dynamics of a foundation rather than model it. In this paper a composite linear model of a super-critical rotor supported on a foundation through ball-bearings is developed using the mechanical impedance technique. Experimental results are presented to validate the model. Gyroscopic effects, although included in the model, were not investigated due to the limitations of the test rig.

1. INTRODUCTION

Rotating machinery in power plants and industry is generally supported on foundation structures that are flexible over the operational speed range and thus contribute to the dynamics of the coupled system. A review of the modelling procedures used for such systems [1] shows that the two major methods employed are the transfer matrix (TM) method and the finite element (FE) method. While the TM method is computationally more efficient than the FE method, its restriction to chain-like structures necessitated the development of the enhanced TM methods [2] and combined FE/TM methods [3] to include the coupled foundation structure. Like the TM method, the mechanical impedance method deals with steady state frequency response descriptions for linear mechanical components. The component is described by a single matrix that incorporates mass, stiffness, damping and gyroscopic terms, relating the forces at the input terminals to the resulting velocities at the output terminals [4]. Similar matrix assembly techniques to those used in FE can be used in the mechanical impedance method. However, in deriving the mechanical impedance matrix of an element analytically using the wave approach, the exact dynamic shape of the element is used [5] rather than the quasi-static approximation used in FE. Hence, provided the element is uniform, its size is unrestricted, with no effect on accuracy. This leads to a much smaller

0022-460X/01/030445 + 22 $35.00/0

number of degrees of freedom compared to the FE method. Consequently, the mechanical impedance technique offers the suitability of FE methods to model coupled rotor-bearing-foundation systems with the advantages of computational efficiency. However, its main advantage relative to the transfer matrix approach is that, unlike the TM method the matrices are formulated directly in terms of frequency-response functions, which can be determined from measurement with very little manipulation. This facilitates a flexible modelling approach. For example, some parts of the rotor dynamic system can be modelled using FE techniques, or the wave approach as discussed in this paper, and some parts of the system could be characterized by measurement. A methodology such as this could be particularly useful when trying to modify a system that has already been built, where it would be much quicker and easier to measure the dynamic behaviour of the foundation rather than to model it. Although there is PC-based proprietary software that will handle complex rotor systems, for example reference [6], it is believed that the system proposed in this paper has some advantages in that it can be easily implemented on standard software, including spreadsheets, with considerable cost saving.

The mechanical impedance method is generally well documented [4, 5], but its application to rotor dynamics problems is relatively unexplored. Reiger *et al.* [7] applied the analogous dynamic stiffness technique to a general rotor-bearing system in order to find its unbalance response, critical speeds and instability threshold speeds. Similar work was done more recently by Raffa *et al.* [8] with respect to unbalance response. However, in both these works foundation flexibility was not included. In the present work, the mechanical impedance formulation was used instead of the dynamic stiffness formulation. However, such a choice is not important since the two formulations merely differ by a factor of $j\omega$.

In this paper the rotor system is split into two, the rotor-bearing subsystem and the foundation subsystem. The rotor-bearing subsystem is modelled as beams, discs and linear springs, and the foundation subsystem, which consists of bearing housings (pedestals), foundation structure and isolation system. Thus, the bearing pedestals are considered to be integral with the foundation, which follows the approach taken by Kramer [9], but is in contrast to the approach taken by Reiger and Zhou [10], where the bearing pedestals are modelled as a separate subsystem. The features of the model described in this paper that set it apart from the models discussed in references [9, 10] are that a hybrid (part analytical model, part experimental model) approach can be used. To illustrate this, two alternative approaches are taken to include foundation flexibility effects in the model. In the first approach, called the *theoretical* model, the foundation subsystem is modelled as a Timoshenko beam, with attached rigid bodies for bearing pedestals and other attachments. Alternatively, it could be modelled by using FE techniques such as in reference [3], and the impedance of the foundation subsystem exported from the FE software into the coupled system model. In the second approach, called the *hybrid* model, the foundation impedance matrix can be determined by measurement. With both approaches the impedance matrix of the foundation subsystem is determined independently from the rotor-bearing subsystem and subsequently integrated into the impedance matrix of the complete rotor-bearing- foundation assembly.

The aim of this paper is to develop an analytical model based on the mechanical impedance technique to predict the unbalance response of a general multi-span coupled rotor-bearing-foundation system and validate it on small-scale test rig. The paper is organised as follows. Following this introduction, the derivation of the model is presented in section 2. The experimental work is described in section 3, the results discussed in section 4 and some conclusions given in section 5.

2. MODEL DEVELOPMENT

2.1. GENERAL DESCRIPTION

The simplified general model used in this paper is shown in Figure 1 where the z-axis is along the shaft, the xz plane is horizontal and the yz plane is vertical. A list of notation is given in Appendix A. This system can be conveniently divided into the rotor-bearing subsystem and the foundation subsystem. The rotor-bearing subsystem has M stations ($i = 1 \cdots M$) that are joined by shaft elements which are modelled as beam segments which can rotate about their longitudinal axis and bend in both xz and yz planes. A rotor station i

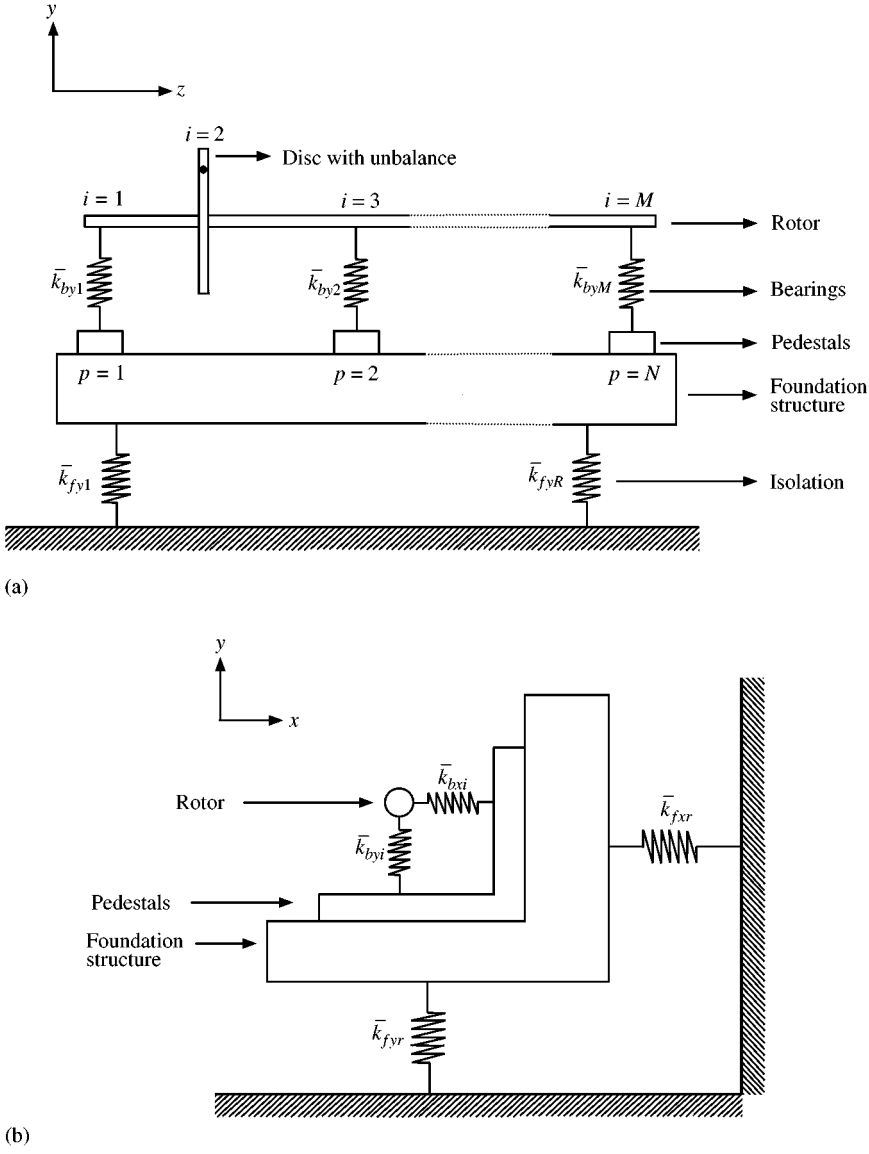

Figure 1. Model adopted for a multi-span coupled rotor-bearing-foundation system. (a) projection on yz plane, (b) general projection on xy plane.

is defined as a location along the rotor where there is either a bearing, a disc, or a change in cross-section. Any out-of-balance is assumed to be concentrated at the discs and internal damping in the shaft is neglected. The shaft segments can be modelled either as rotating Euler–Bernoulli or Timoshenko beams bending in two planes depending on the speed of interest and the size of the shaft. Each bearing (excluding the housing) is modelled as a pair of uncoupled complex (damped) springs in the x and y directions. Such a model is admissible for rolling element bearings but not for journal bearings where strong cross-coupling between the two orthogonal directions exists [11].

2.2. ROTOR-BEARING SUBSYSTEM MODEL

2.2.1. *Impedance matrix of a shaft element*

The shaft element is shown in Figure 2. There is a choice of two shaft elements depending upon the operational speed and type of system to be modelled. An Euler–Bernoulli beam model is appropriate for low-speed flexible shafts and a Timoshenko beam model is appropriate for high-speed, larger diameter shafts. Because the polar moment of inertia is neglected in the Euler–Bernoulli shaft element, the vibrations in the two planes of bending are uncoupled. In this case, the impedance matrix of the shaft element can be determined by simply expanding the impedance matrix of an Euler–Bernoulli beam bending in one plane to include both planes of bending. The relationship between the force and velocity vectors and the impedance matrix of the nth shaft element is given by (a list of notation is given in Appendix A)

$$\mathbf{f}_n = \mathbf{Z}_n \mathbf{v}_n, \tag{1}$$

where $\mathbf{f}_n = [Q_{1n}\, Q'_{1n}\, M_{1n}\, M'_{1n}\, Q_{2n}\, Q'_{2n}\, M_{2n}\, M'_{2n}]^{\mathrm{T}}$, $\mathbf{v}_n = [V_{1n}\, V'_{1n}\, \Omega_{1n}\, \Omega'_{1n}\, V_{2n}\, V'_{2n}\, \Omega_{2n}\, \Omega'_{2n}]^{\mathrm{T}}$ and $\mathbf{Z}_n$ is the 8×8 expanded form of the 4×4 impedance matrix described by Lyon [12] and is given by

$$\mathbf{Z}_n = \begin{bmatrix} a & 0 & b & 0 & c & 0 & d & 0 \\ 0 & a & 0 & b & 0 & c & 0 & d \\ b & 0 & e & 0 & -d & 0 & f & 0 \\ 0 & b & 0 & e & 0 & -d & 0 & f \\ c & 0 & -d & 0 & a & 0 & -b & 0 \\ 0 & c & 0 & -d & 0 & a & 0 & -b \\ d & 0 & f & 0 & -b & 0 & e & 0 \\ 0 & d & 0 & f & 0 & -b & 0 & e \end{bmatrix},$$

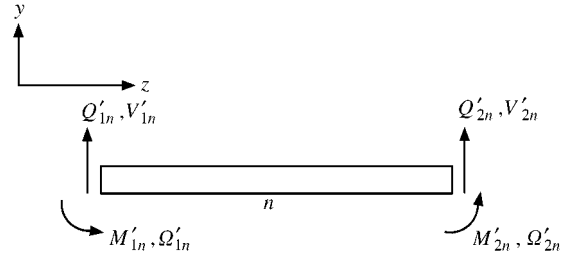

Figure 2. Projection of shaft segment n in yz plane.

where a, b, c, d, e and f for a shaft of length L and cross-sectional area A are given by

$$a = \frac{-\mathrm{j}Jk(\sin kL \cosh kL + \cos kL \sinh kL)}{\Delta}, \quad b = \frac{-\mathrm{j}J \sin kL \sinh kL}{\Delta},$$

$$c = \frac{\mathrm{j}Jk(\sinh kL + \sin kL)}{\Delta}, \quad d = \frac{\mathrm{j}J(\cos kL - \cosh kL)}{\Delta}$$

$$e = \frac{\mathrm{j}J(\cos kL \sinh kL - \sin kL \cosh kL)}{k\Delta}, \quad f = \frac{\mathrm{j}J(\sin kL - \sinh kL)}{k\Delta},$$

where $\Delta = 1 - \cosh kL \cos kL$, $J = \rho A c_l K$, $c_l = \sqrt{E/\rho}$, $K = \sqrt{I/A}$, $k = \omega^{1/2}(\rho A/EI)^{1/4}$.

With a Timoshenko shaft element the inclusion of the polar moment of inertia results in the coupling of the two planes of bending due to the gyroscopic terms. The impedance matrix is thus more complicated and is obtained by solving a pair of equations relating to vibration in the xz and yz planes. The manipulation follows Dimentberg's analysis of a flexible shaft with closely spaced discs attached [13] and differs considerably from the manipulation done by Raffa *et al.* [8]. The equations of motion of the shaft are

$$EI\frac{\partial^4 x}{\partial z^4} - \left\{I_t + m\frac{EI}{\alpha AG}\right\}\frac{\partial^4 x}{\partial z^2 \partial t^2} + m\frac{\partial^2 x}{\partial t^2} + I_t\frac{m}{\alpha AG}\frac{\partial^4 x}{\partial t^4} - I_p\Omega\frac{\partial^3 y}{\partial t \partial z^2} + I_p\Omega\frac{m}{\alpha AG}\frac{\partial^3 y}{\partial t^3} = 0, \tag{2a}$$

$$EI\frac{\partial^4 y}{\partial z^4} - \left\{I_t + m\frac{EI}{\alpha AG}\right\}\frac{\partial^4 y}{\partial z^2 \partial t^2} + m\frac{\partial^2 y}{\partial t^2} + I_t\frac{m}{\alpha AG}\frac{\partial^4 y}{\partial t^4} + I_p\Omega\frac{\partial^3 x}{\partial t \partial z^2} - I_p\Omega\frac{m}{\alpha AG}\frac{\partial^3 x}{\partial t^3} = 0, \tag{2b}$$

where $I_p = 2I_t$. From equations (2a,b) it can be seen that the two planes of bending are coupled by the last two terms on the left-hand sides of equations (2), which are the gyroscopic terms. For harmonic motion at frequency ω,

$$x(z,t) = \mathrm{Re}\{X(z)\mathrm{e}^{\mathrm{j}\omega t}\}, \quad y(z,t) = \mathrm{Re}\{Y(z)\mathrm{e}^{\mathrm{j}\omega t}\}, \tag{3a,b}$$

where $\mathrm{Re}\{\ \}$ denotes the real part of $\{\ \}$ and $X(z)$ and $Y(z)$ are assumed to have the form

$$X(z) = C_1\mathrm{e}^{(\eta/L)z}, \quad Y(z) = C_2\mathrm{e}^{(\eta/L)z}, \tag{4a,b}$$

in which C_1 and C_2 are constants. Combining equations (2–4) results in the matrix equation

$$\begin{bmatrix} \{\eta^4 + \lambda^4(s^2 + r^2)\eta^2 - \lambda^4(1 - s^2r^2\lambda^4)\} & -\mathrm{j}(2/\mu)\lambda^4 r^2(\eta^2 + \lambda^4 s^2) \\ \mathrm{j}(2/\mu)\lambda^4 r^2(\eta^2 + \lambda^4 s^2) & \{\eta^4 + \lambda^4(s^2 + r^2)\eta^2 - \lambda^4(1 - s^2r^2\lambda^4)\} \end{bmatrix} \begin{bmatrix} C_1 \\ C_2 \end{bmatrix} = \begin{bmatrix} 0 \\ 0 \end{bmatrix}, \tag{5}$$

where $\mu = \omega/\Omega$, $s^2 = EI/(\alpha AGL^2)$ is the shear flexibility parameter, $\lambda = kL$ is the non-dimensional Euler–Bernoulli wavenumber and $r^2 = r_0^2/L^2$ is the rotary inertia parameter [5]. To determine the characteristic equation of equation (5), the determinant of the 2×2

matrix is set to zero, which results in the eighth order equation

$$\left[\eta^4 + \lambda^4\left\{s^2 + \left(1 - \frac{2}{\mu}\right)r^2\right\}\eta^2 - \lambda^4\left\{1 - \left(1 - \frac{2}{\mu}\right)s^2r^2\lambda^4\right\}\right]$$

$$\left[\eta^4 + \lambda^4\left\{s^2 + \left(1 + \frac{2}{\mu}\right)r^2\right\}\eta^2 - \lambda^4\left\{1 - \left(1 + \frac{2}{\mu}\right)s^2r^2\lambda^4\right\}\right] = 0. \tag{6}$$

The eight solutions to this equation are $\eta = \pm\eta_a,\ \pm j\eta_b,\ \pm\eta_c,\ \pm j\eta_d$, where

$$\eta_a, \eta_b = \left[\frac{\mp\{s^2 + (1 - 2/\mu)r^2\} + \sqrt{\{s^2 + (1 - 2/\mu)r^2\}^2 + (4/\lambda^4)\{1 - (1 - 2/\mu)s^2r^2\lambda^4\}}}{2}\right]^{1/2}\lambda^2,$$

$$\eta_c, \eta_d = \left[\frac{\mp\{s^2 + (1 + 2/\mu)r^2\} + \sqrt{\{s^2 + (1 + 2/\mu)r^2\}^2 + (4/\lambda^4)\{1 - (1 + 2/\mu)s^2r^2\lambda^4\}}}{2}\right]^{1/2}\lambda^2.$$

A general solution for $X(z)$ and $Y(z)$ is of the form

$$X(z) = A_1H_a\sinh\gamma_az + A_2H_a\cosh\gamma_az - A_3H_b\sin\gamma_bz + A_4H_b\cos\gamma_bz$$
$$+ A_5H_c\sinh\gamma_cz + A_6H_c\cosh\gamma_cz - A_7H_d\sin\gamma_dz + A_8H_d\cos\gamma_dz, \tag{7a}$$

$$Y(z) = c_aA_1H_a\sinh\gamma_az + c_aA_2H_a\cosh\gamma_az - c_bA_3H_b\sin\gamma_bz + c_bA_4H_b\cos\gamma_bz$$
$$+ c_cA_5H_c\sinh\gamma_cz + c_cA_6H_c\cosh\gamma_cz - c_dA_7H_d\sin\gamma_dz + c_dA_8H_d\cos\gamma_dz, \tag{7b}$$

where $\gamma_a = \gamma(\eta_a), \gamma_b = \gamma(\eta_b), \gamma_c = \gamma(\eta_c), \gamma_d = \gamma(\eta_d)$, where $\gamma(\eta) = \eta/L$; $H_a = H(\gamma_a), H_b = H(\gamma_b)$, $H_c = H(\gamma_c)$, $H_d = H(\gamma_d)$, where $H(\gamma) = \gamma/(\rho A\omega^2)$; $c_a = c(\eta_a^2)$, $c_b = c(-\eta_b^2)$, $c_c = c(\eta_c^2)$, $c_d = c(-\eta_d^2)$, where $c(\eta^2) = C_2/C_1 = \pm j$, determined from equation (5); and A_1–A_8 are arbitrary constants. Similar expressions for $\theta_x(z)$, $\theta_y(z)$, $Q_x(z)$, $Q_y(z)$, $M_x(z)$, $M_y(z)$, respectively, can be obtained [14]:

$$\theta_x(z) = A_1J_a\cosh\gamma_az + A_2J_a\sinh\gamma_az + A_3J_b\cos\gamma_bz + A_4J_b\sin\gamma_bz$$
$$+ A_5J_c\cosh\gamma_cz + A_6J_c\sinh\gamma_cz + A_7J_d\cos\gamma_dz + A_8J_d\sin\gamma_dz, \tag{7c}$$

$$\theta_y(z) = c_aA_1J_a\cosh\gamma_az + c_aA_2J_a\sinh\gamma_az + c_bA_3J_b\cos\gamma_bz + c_bA_4J_b\sin\gamma_bz$$
$$+ c_cA_5J_c\cosh\gamma_cz + c_cA_6J_c\sinh\gamma_cz + c_dA_7J_d\cos\gamma_dz + c_dA_8J_d\sin\gamma_dz, \tag{7d}$$

$$Q_x(z) = A_1\cosh\gamma_az + A_2\sinh\gamma_az + A_3\cos\gamma_bz + A_4\sin\gamma_bz$$
$$+ A_5\cosh\gamma_cz + A_6\sinh\gamma_cz + A_7\cos\gamma_dz + A_8\sin\gamma_dz, \tag{7e}$$

$$Q_y(z) = c_a A_1 \cosh \gamma_a z + c_a A_2 \sinh \gamma_a z + c_b A_3 \cos \gamma_b z + c_b A_4 \sin \gamma_b z + c_c A_5 \cosh \gamma_c z + c_c A_6 \sinh \gamma_c z + c_d A_7 \cos \gamma_d z + c_d A_8 \sin \gamma_d z, \tag{7f}$$

$$M_x(z) = EI\{A_1 \gamma_a J_a \sinh \gamma_a z + A_2 \gamma_a J_a \cosh \gamma_a z - A_3 \gamma_b J_b \sin \gamma_b z + A_4 \gamma_b J_b \cos \gamma_b z + A_5 \gamma_c J_c \sinh \gamma_c z + A_6 \gamma_c J_c \cosh \gamma_c z - A_7 \gamma_d J_d \sin \gamma_d z + A_8 \gamma_d J_d \cos \gamma_d z\}, \tag{7g}$$

$$M_y(z) = EI\{c_a A_1 \gamma_a J_a \sinh \gamma_a z + c_a A_2 \gamma_a J_a \cosh \gamma_a z - c_b A_3 \gamma_b J_b \sin \gamma_b z + c_b A_4 \gamma_b J_b \cos \gamma_b z + c_c A_5 \gamma_c J_c \sinh \gamma_c z + c_c A_6 \gamma_c J_c \cosh \gamma_c z - c_d A_7 \gamma_d J_d \sin \gamma_d z + c_d A_8 \gamma_d J_d \cos \gamma_d z\}, \tag{7h}$$

in which

$J_a = J(\eta_a^2)$, $J_b = J(-\eta_b^2)$, $J_c = J(\eta_c^2)$, $J_d = J(-\eta_d^2)$ where

$$J(\eta^2) = (L^2/EI)\{s^2 + \eta^2/\lambda^4\}.$$

Applying the displacement boundary conditions

$$\text{at } x = \begin{cases} 0\text{: } X(z) = X_{1n}, & Y(z) = Y_{1n}, & \theta_x(z) = \theta_{1n}, & \theta_y(z) = \theta'_{1n}, \\ L\text{: } X(z) = X_{2n}, & Y(z) = Y_{2n}, & \theta_x(z) = \theta_{2n}, & \theta_y(z) = \theta'_{2n}, \end{cases}$$

to equations (7a–d) gives

$$\mathbf{u}_n = \mathbf{P}_1 \mathbf{a}, \tag{8a}$$

where

$$\mathbf{u}_n = [X_{1n}\ Y_{1n}\ \theta_{1n}\ \theta'_{1n}\ X_{2n}\ Y_{2n}\ \theta_{2n}\ \theta'_{2n}]^{\mathrm{T}}$$

$$\mathbf{a} = [A_1\ A_2\ A_3\ A_4\ A_5\ A_6\ A_7\ A_8]^{\mathrm{T}}$$

and $\mathbf{P}_1$ is an 8×8 matrix. Applying the force/moment boundary conditions

$$\text{at } x = \begin{cases} 0\text{: } Q_x(z) = Q_{1n}, & Q_y(z) = Q'_{1n}, & M_x(z) = -M_{1n}, & M_y(z) = M'_{1n}, \\ L\text{: } Q_x(z) = -Q_{2n}, & Q_y(z) = -Q'_{2n}, & M_x(z) = M_{2n}, & M_y(z) = M'_{2n}, \end{cases}$$

to equations (7e–h) gives

$$\mathbf{f}_n = \mathbf{P}_2 \mathbf{a}, \tag{8b}$$

where $\mathbf{f}_n = [Q_{1n}\ Q'_{1n}\ M_{1n}\ M'_{1n}\ Q_{2n}\ Q'_{2n}\ M_{2n}\ M'_{2n}]^{\mathrm{T}}$ and $\mathbf{P}_2$ is an 8×8 matrix. Eliminating $\mathbf{a}$ from equations (8a,b) gives

$$\mathbf{f}_n = \mathbf{P}_2 \mathbf{P}_1^{-1} \mathbf{u}_n \tag{9}$$

and hence the impedance matrix $\mathbf{Z}_n$ of the rotating Timoshenko shaft element is given by

$$\mathbf{Z}_n = \mathbf{P}_2\mathbf{P}_1^{-1}/(\mathrm{j}\omega). \tag{10}$$

2.2.2. *Assembly of rotor-bearing subsystem impedance matrix*

The impedance matrices of consecutive shaft elements are assembled in a manner similar to that of FE [11], by using continuity of linear and angular velocities at each shaft station. An example of the assembly of two consecutive shaft elements is shown in Figure 3. For a total of M rotor stations, the assembled rotor-bearing subsystem matrix, $\mathbf{Z}_r$, is of order $4M \times 4M$ where

$$\mathbf{f} = \mathbf{Z}_r\mathbf{v}_r \tag{11}$$

and $\mathbf{v}_r = [V_1\ V_1'\ \Omega_1\ \Omega_1' \cdots V_M\ V_M'\ \Omega_M\ \Omega_M']^{\mathrm{T}}$, where $\mathbf{f}_r$ is the column vector of forces external to the rotor-bearing subsystem including the effects of out-of-balance and foundation movement. Additional matrices are added at the appropriate locations to allow for the presence of discs or bearings at the rotor stations. At a disc station the forces and moments are summed in the xz plane, respectively,

$$Q_{2n} + Q_{1(n+1)} = -\mathrm{j}\omega m_i V_i + U_i\Omega^2 \mathrm{e}^{\mathrm{j}\phi_i}, \tag{12a}$$

$$M_{2n} + M_{1(n+1)} = -\mathrm{j}\omega I_{Ti}\Omega_i - I_{Pi}\Omega\Omega_i', \tag{12b}$$

and similarly, in the yz plane one obtains

$$Q_{2n}' + Q_{1(n+1)}' = -\mathrm{j}\omega m_i V_i' + U_i\Omega^2 \mathrm{e}^{\mathrm{j}(\phi_i - \pi/2)}, \tag{13a}$$

$$M_{2n}' + M_{1(n+1)}' = -\mathrm{j}\omega I_{Ti}\Omega_i' + I_{Pi}\Omega\Omega_i, \tag{13b}$$

where ϕ_i is the angular position of the out-of-balance of the disc at station i at time $t = 0$, $U_i = m_i' \times e_i$, is the unbalance of disc at station i where m_i' is the out-of-balance mass and e_i is the eccentricity of m_i'. From equations (12b) and (13b) it is again seen that the two planes

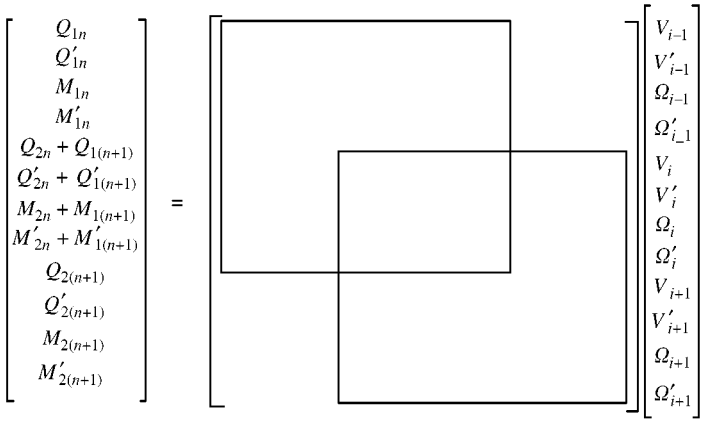

Figure 3. Assembly of impedance matrices of two consecutive shaft segments n, $n + 1$.

of bending are coupled by the gyroscopic terms. If at the ith rotor station there is then a disc:

(a) the matrix

$$\begin{bmatrix} j\omega m_i & 0 & 0 & 0 \\ 0 & j\omega m_i & 0 & 0 \\ 0 & 0 & j\omega I_{Ti} & I_{Pi}\Omega \\ 0 & 0 & -I_{Pi}\Omega & j\omega I_{Ti} \end{bmatrix}$$

is added to the $\{1+4(i-1)\}\cdots\{4+4(i-1)\}$th rows, $\{1+4(i-1)\}\cdots\{4+4(i-1)\}$th columns of the assembled impedance matrix of the rotor; (b) the terms $U_i\Omega^2 e^{j\phi_i}$, $U_i\Omega^2 e^{j(\phi_i-\pi/2)}$ become the $\{1+4(i-1)\}$th, $\{2+4(i-1)\}$th elements of the rotor-forcing vector $\mathbf{f}_r$.

At a bearing station the forces are summed in the x and y directions, respectively,

$$Q_{2n} + Q_{1(n+1)} = z_{bxxi}(V_{fp} - V_i), \tag{14a}$$

$$Q'_{2n} + Q'_{1(n+1)} = z_{byyi}(V'_{fp} - V'_i), \tag{14b}$$

where $z_{bxxi} = \bar{k}_{bxi}/(j\omega)$, $z_{byi} = \bar{k}_{byi}/(j\omega)$ and V_{fp}, V'_{fp} are the velocities of the foundation in the x and y directions, respectively, at the pth bearing pedestal, $(p = 1, \ldots, N)$. Hence, if at the ith rotor station there is the pth bearing, then

(a) the bearing impedance matrix

$$\mathbf{Z_B} = \begin{bmatrix} z_{bxxi} & 0 \\ 0 & z_{byyi} \end{bmatrix} \tag{15}$$

is added to the $\{1+4(i-1)\}\cdots\{2+4(i-1)\}$th rows, $\{1+4(i-1)\}\cdots\{2+4(i-1)\}$th columns of the assembled impedance matrix of the rotor; (b) the terms $z_{bxxi}V_{fp}$, $z_{byyi}V'_{fp}$ become the $\{1+4(i-1)\}$th, $\{2+4(i-1)\}$th elements of the rotor forcing vector $\mathbf{f}_r$.

2.3. FOUNDATION SUBSYSTEM

Since the force inputs from the rotor-bearing subsystem to the foundation assembly are located at the bearings, which are assumed to exert no restraining moment, the foundation impedance matrix can be expressed as a $2N \times 2N$ matrix $\mathbf{Z}_f$ where

$$\mathbf{f}_f = \mathbf{Z}_f \mathbf{v}_f, \tag{16}$$

with $\mathbf{f}_f = [F_{f1}\ F'_{f1} \cdots F_{fN}\ F'_{fN}]^T$ being the vector of forces at the bearing pedestals, and $\mathbf{v}_f = [V_{f1}\ V'_{f1} \cdots V_{fN} V'_{fN}]^T$ the vector of velocities at the N bearing pedestals. Note that no external moments and angular velocities are included in the above formulation since the former are assumed to be zero and the later are not required. In the hybrid model approach $\mathbf{Z}_f$ is determined empirically or by means other than the mechanical impedance technique.

To obtain the matrix $\mathbf{Z}_f$ by using the theoretical model, the foundation impedance matrix is first assembled in a manner similar to that of the rotor-bearing system. However, the two planes of bending are uncoupled and the impedance matrices of the foundation in the xz and yz planes can be determined separately, resulting in lower order matrices. The impedance matrix for a Timoshenko beam bending in one plane is derived by setting $\Omega = 0$

in equations (2a,b), but with taking note of the different second moments of areas in the two planes of bending. Thus, equation (5) degenerates to,

$$\eta^4 + \lambda^4(s^2 + r^2)\eta^2 - \lambda^4(1 - s^2r^2\lambda^4) = 0 \tag{17}$$

which has roots for bending in either plane $\eta = \pm \eta_a, \ \pm \mathrm{j}\eta_b$, where

$$\eta_a = \left\{\frac{-(s^2 + r^2) + \sqrt{(s^2 - r^2)^2 + 4/\lambda^4}}{2}\right\}^{1/2} \lambda^2,$$

$$\eta_b = \left\{\frac{(s^2 + r^2) + \sqrt{(s^2 - r^2)^2 + 4/\lambda^4}}{2}\right\}^{1/2} \lambda^2.$$

Applying the displacement and force/moment boundary conditions at the nodes in a similar way to that described in section 2.2, gives the impedance matrix for the xz plane

$$\mathbf{Z} = \mathbf{P}_2\mathbf{P}_1^{-1}/(\mathrm{j}\omega), \tag{18}$$

where

$$\mathbf{P}_1 = \begin{bmatrix} 0 & H_a & 0 & H_b \\ J_a & 0 & J_b & 0 \\ H_a \sinh \gamma_a L & H_a \cosh \gamma_a L & -H_b \sin \gamma_b L & H_b \cos \gamma_b L \\ J_a \cosh \gamma_a L & J_a \sinh \gamma_a L & J_b \cos \gamma_b L & J_b \sin \gamma_b L \end{bmatrix},$$

and

$$\mathbf{P}_2 = \begin{bmatrix} 1 & 0 & 1 & 0 \\ 0 & -EI_y\gamma_a J_a & 0 & -EI_y\gamma_b J_b \\ -\cosh \gamma_a L & -\sinh \gamma_a L & -\cos \gamma_b L & -\sin \gamma_b L \\ EI_y\gamma_a J_a \sinh \gamma_a L & EI_y\gamma_a J_a \cosh \gamma_a L & -EI_y\gamma_b J_b \sin \gamma_b L & EI_y\gamma_b J_b \cos \gamma_b L \end{bmatrix}.$$

By following the procedure given in section 2.2 the foundation impedance matrix in one plane is assembled using the continuity of linear and angular velocity at a common station and the insertion of the impedance matrices of the attached masses and isolators at the appropriate location. The resulting assembled foundation impedance matrix $\mathbf{Z}_{Fx}$ in one plane (e.g., the xz plane) is of the form

$$\mathbf{f}_x = \mathbf{Z}_{Fx}\mathbf{v}_x, \tag{19}$$

where $\mathbf{f}_x = [F_{f1} \ M_{f1} \ F_{f2} \ M_{f2} \cdots F_{fR} \ M_{fR}]^{\mathrm{T}}$ is the column vector of external forces and moments on the foundation in the xz plane, and $\mathbf{v}_x = [V_{f1} \ \Omega_{f1} \ V_{f2} \ \Omega_{f2} \cdots V_{fR} \ \Omega_{fR}]^{\mathrm{T}}$ is the column vector of linear and angular velocities in the xz plane at the foundation stations. R is the total number of foundation stations ($N < R$, where N is the number of bearing pedestals). Since external forces on the foundation assembly are only applied at the bearing pedestals, and the angular velocities at the foundation stations are not required, matrix $\mathbf{Z}_{Fx}$ may be reduced to an $N \times N$ matrix, $\mathbf{Z}_{fx}$. This is achieved first by applying the exact static reduction technique that is used in finite element statics to remove all the rotational

co-ordinates from the static stiffness matrix [11]. The resulting matrix is then inverted and the qth row and qth column are deleted, where q is the number of a foundation station at which there is no bearing pedestal attached (and hence no external applied force). The resulting matrix is then re-inverted back to yield $\mathbf{Z}_{fx}$. A similar process is applied to the foundation movement in the yz plane to give $\mathbf{Z}_{fy}$. The two matrices $\mathbf{Z}_{fx}$ and $\mathbf{Z}_{fy}$ are then combined to give the matrix $\mathbf{Z}_f$ as in equation (16).

2.4. THE COUPLED SYSTEM

The $2N \times 1$ foundation forcing vector $\mathbf{f}_f$ in equation (16) contains the forces exerted by the bearings on the foundation: i.e.,

$$\mathbf{f}_f = [z_{bxx1}(V_{f1} - V_1)\ z_{byy1}(V'_{f1} - V'_1) \cdots z_{bxxN}(V_{fN} - V_N)\ z_{byyN}(V'_{fN} - V'_N)]^{\mathrm{T}}. \quad (20)$$

Hence equation (16) can be written as

$$\mathbf{f}_f = \mathbf{Z}'_f \mathbf{v}_f, \quad (21)$$

where $\mathbf{f}_f = [z_{bxx1} V_1\ z_{byy1} V'_1 \cdots z_{bxxN} V_N\ z_{byyN} V'_N]^{\mathrm{T}}$ and $\mathbf{Z}'_f = \mathbf{Z}_f + \mathbf{\Lambda}_f$ where $\mathbf{\Lambda}_f$ is a $2N \times 2N$ diagonal matrix of bearing impedances given by

$$\mathbf{\Lambda}_f = \begin{bmatrix} z_{bxx1} & & & & & \\ & z_{byy1} & & & & \\ & & \ddots & & & \\ & & & z_{bxxN} & & \\ & & & & z_{byyN} & \end{bmatrix}. \quad (22)$$

The final step in assembling the overall impedance matrix $\mathbf{Z}$ of the coupled rotor-bearing-foundation assembly is the integration of the system of equations given by equation (11) for the rotor-bearing subsystem and equation (21) for the bearing-foundation subsystem. The final result is found to be

$$\mathbf{f} = \mathbf{Z}\mathbf{v}, \quad (23)$$

where $\mathbf{v} = [V_1\ V'_1\ \Omega_1\ \Omega'_1 \cdots V_M\ V'_M\ \Omega_M\ \Omega'_M\ V_{f1}\ V'_{f1} \cdots V_{fN}\ V'_{fN}]^{\mathrm{T}}$ and

$$\mathbf{Z} = \begin{bmatrix} \mathbf{Z}_r & \mathbf{Z}_g \\ \mathbf{Z}_g^{\mathrm{T}} & \mathbf{Z}'_f \end{bmatrix},$$

$\mathbf{Z}$ is of the order $(4M + 2N) \times (4M + 2N)$ and $\mathbf{Z}_r$ and $\mathbf{Z}'_f$ are the assembled rotor-bearing and bearing-foundation matrices given in equations (11) and (21) respectively. $\mathbf{Z}_g$ is a $4M \times 2N$ matrix which contains zeros everywhere except at entries which are filled in according to the following algorithm.

If the pth bearing ($p = 1, \ldots, N$) is at the ith rotor station then insert the matrix $-\mathbf{Z}_B$ at the $\{1 + 4(i-1)\} \cdots \{2 + 4(i-1)\}$th rows, $\{4M + 1 + 2(p-1)\} \cdots \{4M + 2 + 2(p-1)$th columns of $\mathbf{Z}$.

$\mathbf{f}$ is a column vector of forces external to the rotor-bearing-foundation system of length $(4M + 2N)$ which is constructed according to the following algorithm: (a) form a column

vector of zeros of length $(4M + 2N)$; (b) if, at the ith rotor station there is a disc add (i) $U_i\Omega^2 e^{j\phi_i}$ to the $\{1 + 4(i-1)\}$th row, (ii) $U_i\Omega^2 e^{j(\phi_i - \frac{\pi}{2})}$ to the $\{2 + 4(i-1)\}$th row.

Apart from the assumption that there are no restraining moments at the bearings, the above algorithm for $\mathbf{f}$ is valid if there are are no shear force and bending moments in the two planes of bending at the ends of the rotor.

2.5. EXTENSION TO FLUID FILM JOURNAL BEARINGS

The model described above can be extended to linearized fluid film journal bearings by generalizing the matrices $\mathbf{Z_B}$ and $\mathbf{\Lambda}_f$ in equations (15) and (22) to include the cross-coupled bearing impedance terms z_{bxyi}, z_{byxi}, as follows:

$$\mathbf{Z_B} = \begin{bmatrix} z_{bxxi} & z_{bxyi} \\ z_{byxi} & z_{byyi} \end{bmatrix}, \tag{15a}$$

$$\mathbf{\Lambda}_f = \begin{bmatrix} z_{bxx1} & z_{bxy1} & & & & \\ z_{byx1} & z_{byy1} & \ddots & & & \\ & \ddots & \ddots & \ddots & & \\ & & \ddots & z_{bxxN} & z_{bxyN} \\ & & & z_{byxN} & z_{byyN} \end{bmatrix}. \tag{22a}$$

2.6. UNBALANCE RESPONSE, NATURAL FREQUENCIES, INSTABILITY ANALYSIS

For the unbalance response, synchronous vibration applies, i.e., $\omega = \Omega$. $\mathbf{Z}$ and $\mathbf{f}$ in equation (23) are determined for each speed and $\mathbf{Z}$ inverted to give $\mathbf{v}$ and hence the deflection vector $\mathbf{u} = \mathbf{v}/(j\omega)$. Thus the unbalance response at each rotor station and bearing pedestal can be obtained. Moreover, for any speed, once $\mathbf{u}$ has been determined, the complex amplitudes X, Y of the deflections at any *arbitrary* location P along the rotor can be determined *exactly* [14]. The shaft orbit at P can be obtained for any speed by forming the complex number $w(t) = x(t) + jy(t)$, where $x(t) = \mathrm{Re}\{Xe^{j\omega t}\}$, $y(t) = \mathrm{Re}\{Ye^{j\omega t}\}$ and plotting $w(t)$ on an Argand diagram from $t = 0$ to $2\pi/\omega$. From the sense of rotation of this plot about the origin it can established whether the whirl is of the forward or reverse type at that speed. The critical speeds are obtained directly from the maxima of the unbalance response.

The rotor and bearing pedestal velocities given by equation (23) are *absolute* values, measured with respect to an inertial frame of reference. In practice, absolute accelerations of bearing pedestal vibrations are generally measured. However, for rotor deflections, proximity probes are more frequently used, which give the deflections of the shaft relative to the foundation. For positions P on the rotor and Q on the foundation the relative displacements are given by

$$X_r = X_P - X_Q, \quad Y_r = Y_P - Y_Q, \tag{24a,b}$$

where X_P, Y_P, X_Q, Y_Q are absolute values. Equations (24a,b) essentially neglect any "wobbling" of the foundation about the z-axis. If P and Q are not located at a bearing pedestal a "dummy" bearing pedestal of zero bearing stiffness and damping and zero pedestal mass can be inserted between P and Q as shown in Figure 4. X_P, Y_P, X_Q, Y_Q will then be obtained directly from equation (23).

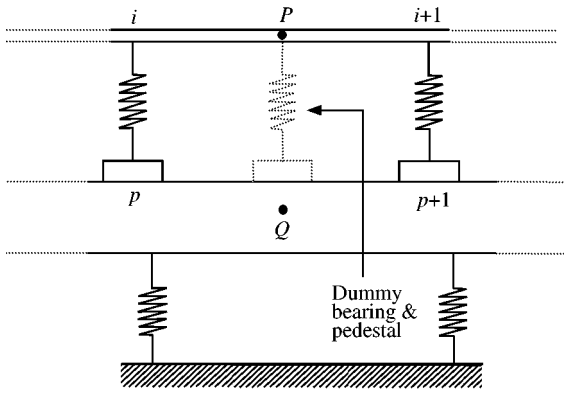

Figure 4. Insertion of dummy bearing and pedestal for the determination of relative motion.

For the determination of the natural frequencies and instability threshold speeds, general (non-synchronous) vibration conditions are considered. The natural frequencies ω_n at each speed Ω are found by locating the zeros of the determinant of the impedance matrix $\mathbf{Z}$ of the system and taking their real part. The instability threshold speeds could also be found by observing the speeds where the imaginary part of these zeros changes sign. The zeros of the determinant of $\mathbf{Z}$ are located by using Muller's Algorithm as in reference [7]. The critical speeds can also be obtained by finding where the speed Ω is equal to a natural frequency. Since the aim of the paper was to present and validate a simple method of linking the foundation subsystem with the rotor-bearing subsystem, the prediction of natural frequencies and instability threshold speeds was considered outside the scope of this research, which was restricted to the determination of the unbalance response and critical speeds from the maxima. Moreover, instability problems arise due to the cross-coupled bearing impedance terms z_{bxyi}, z_{byxi} [11] which are significant in fluid film journal bearings but negligible in rolling element bearings, as previously mentioned.

3. MODEL VALIDATION

3.1. DESCRIPTION OF TEST RIG

The test rig used for the experimental verification of the coupled rotor-bearing-foundation system model is shown in Figure 5. It was a modification of a Bentley Nevada Rotor Kit *RK*4 and consisted of a mild steel 10 mm diameter shaft mounted on three nominally identical double-row self-aligning ball bearings housed in three mild steel-bearing pedestals *BP*1, *BP*2 and *BP*3. The shaft carried a 30 mm diameter steel disc termed the *rotor mass wheel W*, into which known unbalance masses could be screwed. The shaft was connected to the motor *M* via a flexible coupling. The foundation, which was entirely made of an aluminium alloy consisted of a right-angled "V" section beam with three feet *F*1, *F*2, *F*3 attached. The whole assembly was supported by a thick layer of foam to provide suitable isolation.

With reference to Figure 6 the model developed in the previous section was used to solve two model problems, over a rotational speed range of 1500–12 000 rpm with a resolution of 30 rpm. The first problem (Problem I) was to find the absolute unbalance response at the bearing pedestals *BP*1, *BP*2, *BP*3 and at positions P_1–P_6 along the rotor by both the

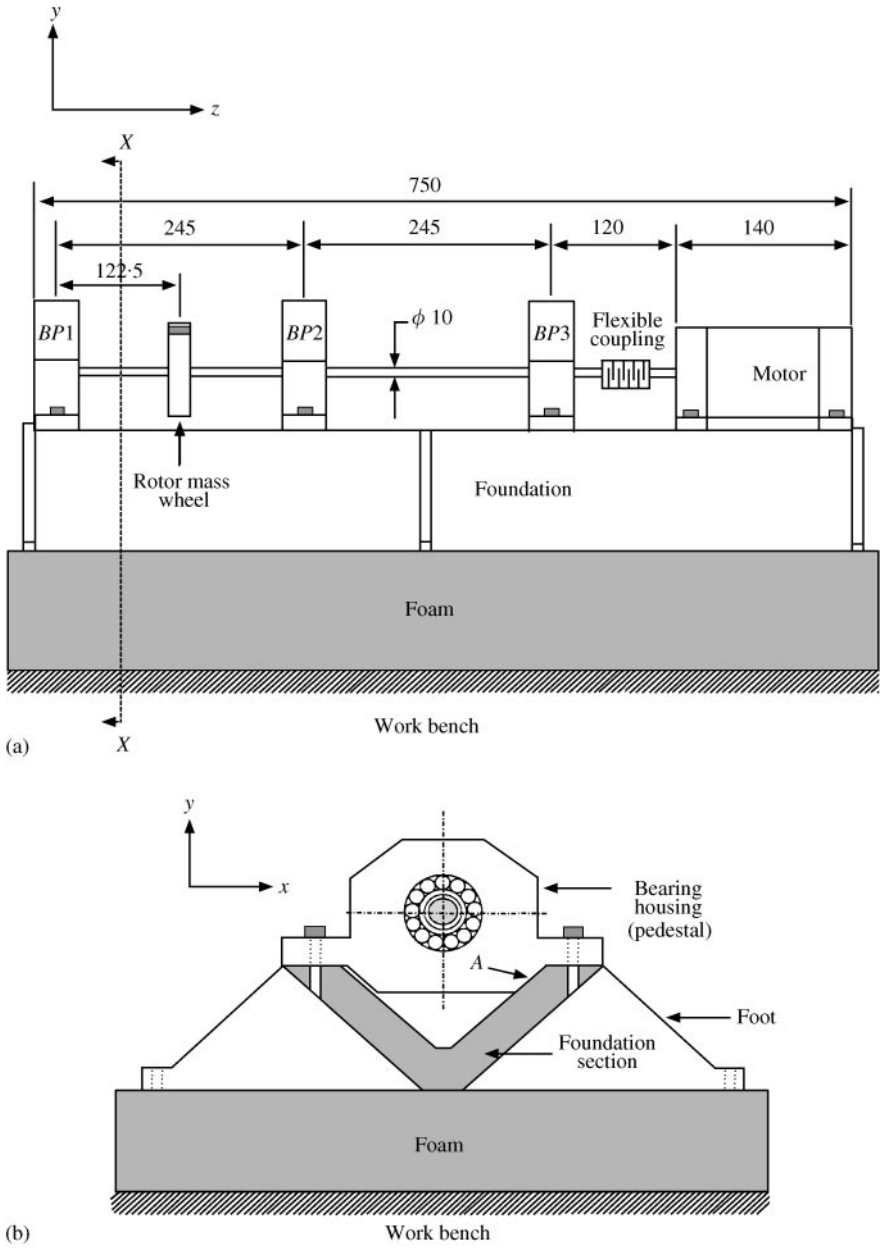

Figure 5. Coupled rotor-bearing-foundation system test rig (*all dimensions in* mm). (a) Side elevation, (b) View on Section X–X.

theoretical and the hybrid models, and the second problem (Problem II) was to determine the unbalance response of the points P_3 and P_5 on the rotor relative to the foundation by the theoretical model only. In the both problems the simulation made use of single, speed-independent estimates for bearing stiffness (2 MN/m) and loss factor (0·2) for both the x and y directions obtained by simple static tests, and which hence neglected any effect of ball bearing rotation [11]. For the theoretical model solution the foundation subsystem was modelled as a *floating* Timoshenko beam with attached rigid bodies as shown in Figure 7. The reason for this was that for frequencies well above the fundamental frequency of the

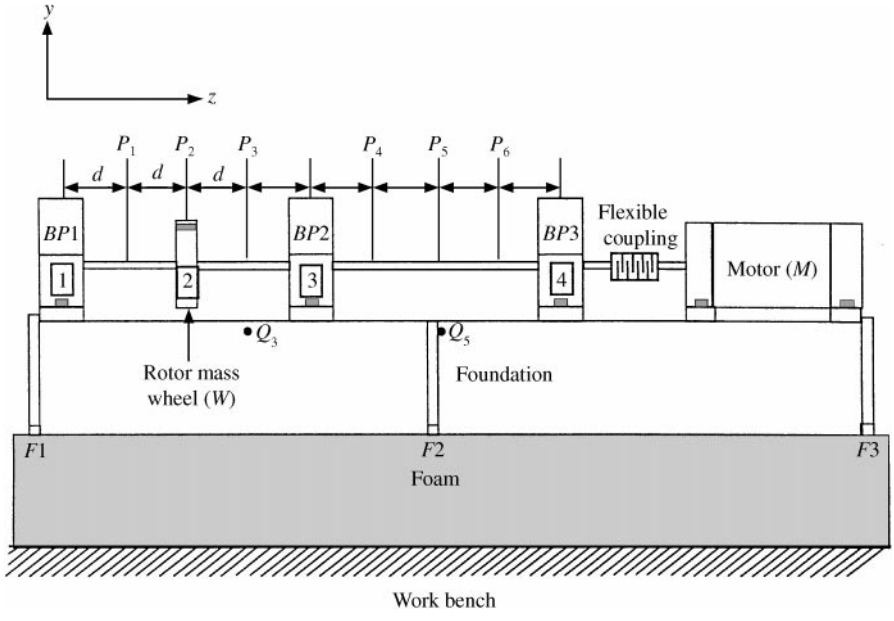

Figure 6. Test-rig set-up for the solution and experimental verification of Problem I (d = 61·25 mm).

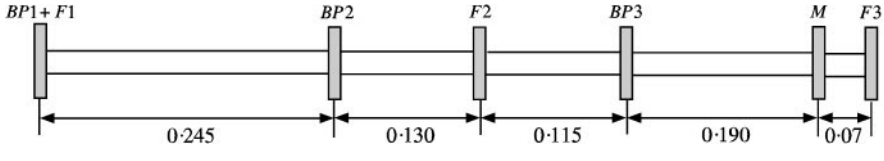

Figure 7. Simplified model of the foundation subsystem shown in Figure 6 (*all dimension in* m).

isolation (somewhere in the range 5–20 Hz) the presence of the isolation can be neglected and the supported structure behaves as if floating freely in space [14]. The mass and moment of inertia of each body (including the motor) were assumed to be concentrated at the axial position (i.e., position along the z-axis) of the centre of mass of the body. For the solution of Problem II dummy bearings were added between P_3 and Q_3 and between P_5 and Q_5. The simulations are compared with experimental results in section 4.

3.2. EXPERIMENTAL WORK

For the hybrid model the dynamic response of the foundation was required and this was measured by using impact hammer excitation. Measurements were performed separately for the vertical and horizontal planes. For these tests the rotor assembly was removed but the bearings were retained in their pedestals. Strictly speaking, the bearings should have been removed since they formed part of the rotor-bearing subsystem. However, their removal would have affected their pre-load which in turn would alter their stiffness value which had been previously measured. Because the mass of the bearings was less than 1/20th of the bearing pedestal assembly mass the error introduced by retaining the bearings was considered to be negligible. For all the tests a frequency range of 0–200 Hz and a resolution of 0·5 Hz was used.

Time constraints did not allow for the quantification of the residual unbalance due to geometric inaccuracies in the disc and the lack of straightness of the machined shaft. Hammer tests were therefore conducted on the *stationary* rig, enabling verification of the predicted unbalance response curves for the two model problems over the speed range 1500–12 000 rpm. When using an impact hammer on the wheel W in the x direction, the transfer accelerance between W and an arbitrary location P on the system, $a_{PW_x} = A_x/F_x$ can be measured, where A_x is the acceleration at P due to the force F_x. Now in rotation, $F_x = U\omega^2$ and hence $a_{PW_x} = A_x/U\omega^2 = -X/U$ where $X = -A_x/\omega^2$ is the displacement at P in the x direction due to the unbalance U at W. Similarly, for an impact at W in the y direction the transfer accelerance between P and W is found to be $a_{PW_y} = -Y/(U\mathrm{e}^{-j\frac{\pi}{2}})$. Hence, it is seen that the magnitudes of the frequency response functions a_{PW_x} and a_{PW_y}, respectively, give the displacement responses at P in the x and y directions for unit unbalance at the wheel W. Hence, by using an unbalance of 1 kg in the simulations the results can be directly compared with the measured accelerances discussed above.

For validation of the first problem three accelerometers were attached to points P_1, P_2, P_3 shown in Figure 6 with their sensitivity axes along the y direction and a hammer blow was applied at W in the y direction. The accelerances between W and P_1, P_2, P_3 were measured. This procedure was repeated with at P_4, P_5, P_6 and again at the bearing pedestals $BP1$, $BP2$, $BP3$. A similar procedure was then repeated for the x direction. For the validation of the second problem two accelerometers were attached at points P_3 and Q_3, respectively, with their main sensitivity axes along the y direction, and the accelerances between W and P_3, Q_3 were measured. The difference between these two accelerances gives the y displacement response of P_3 relative to Q_3 for unit unbalance at W. This procedure was repeated for P_5 and Q_5 respectively. A similar procedure was then repeated for the x direction.

The use of hammer tests on the stationary test rig to determine the unbalance response of the rotating system is justified provided (a) the behaviour of the ball bearings is unaffected by rotation, and (b) the vibrations in the x and y directions during rotation are uncoupled, i.e., the gyroscopic effects due to the polar moment of inertia of the disc and the shaft are negligible. Subject to these conditions, the measured resonance frequencies of a stationary system can be considered as the critical speeds of the rotating system. Assumption (b) is justified by noting that the polar moment of inertia of the wheel, at $0{\cdot}5660 \times 10^{-3}$ kg m^2 was negligible. Needless to say, the distributed polar moment of inertia of the slender 10 mm diameter shaft was even more negligible. As regards assumption (a), it is observed in reference [11] that ball-bearings exhibit non-linearities in rotation. Hence, the static hammer tests for this particular case study are adequate to verify all aspects of the model except the assumption of linear behaviour of the bearings in rotation.

The instantaneous displacements in the x and y directions at P_3 for 18 different speeds in the range 1500–6000 rpm were measured by using Bentley Nevada $RK4$ proximity probes $P1$ and $P2$ mounted in the respective directions at point P_3. The sampling frequency was 4096 Hz and the record length 0·125 s. The measured orbits were constructed from the x and y displacements and show the motion of the shaft at P_3 during an interval of 0·125 s.

4. RESULTS AND DISCUSSION

Figure 8a–8d show the simulation results for the first problem obtained by using the *theoretical* model for the absolute unbalance response at rotor position P_3 (Figures 8(a,b)) and at bearing pedestal $BP2$ (Figures 8(c,d)) in the x and y directions. The hammer test measurements are overlaid on the same axes. From these figures it can be seen that there is

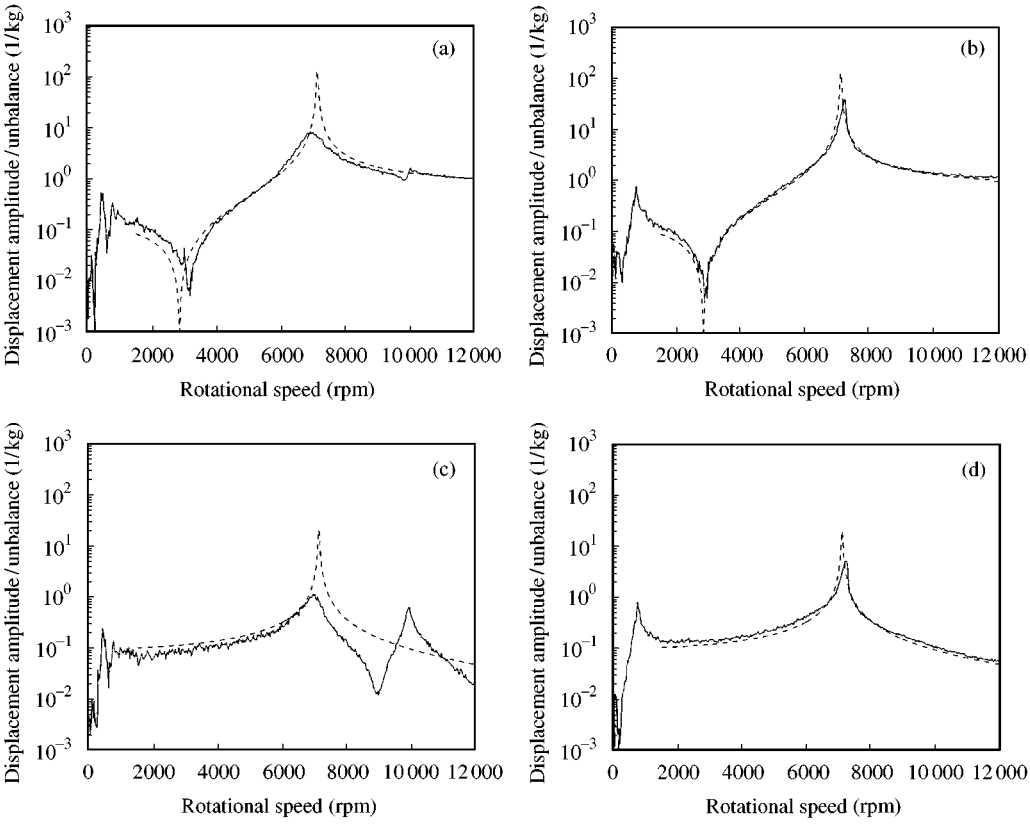

Figure 8. Absolute unbalance response in x and y directions at point P_3 and bearing pedestal No. 2 ($BP2$): predictions from *theoretical* model compared with measurement (hammer test). (a) Unbalance response at P_3 in x direction, (b) Unbalance response at P_3 in y direction, (c) Unbalance response at $BP2$ in x direction, (d) Unbalance response at $BP2$ in y direction. ——, hammer test; – – – theoretical model.

good agreement between predictions and measurement in the y direction. The measured critical speed in the y direction (7281 rpm) is slightly *higher* than the predictions from the theoretical model (7161 rpm). The agreement is not so good in the x direction, especially for the response at the bearing pedestal $BP2$ beyond 7000 rpm. In particular, the theoretical model fails to predict a second critical speed measured at 10010 rpm. This speed corresponds to a frequency of 167 Hz which was found to correspond to the first torsional mode of the foundation. In fact, while the y-forces on the bearings of the coupled system induce pure bending on the foundation beam, the x-forces will induce torsion in addition to bending since their lines of action do not pass through the shear centre of the foundation beam section. Moreover, the bending vibrations of the foundation in the xz plane will be coupled with the torsional vibrations since the shear centre and the centroid of the foundation beam section do not coincide [15]. The theoretical model ignores this torsion effect completely. It can be seen in Figures 9(a–d) that the shortcomings of the theoretical model with respect to the absolute response in the x direction, are overcome by the hybrid model, which predicts critical speeds at 7025 and 10191 rpm.

The relative motion at P_3 predicted by the theoretical model is shown in Figures 10(a,b) with the hammer test measurements overlaid on the same axes. There is good agreement between the predicted and measured relative response in the y direction, but not as good agreement as in the x direction. By comparing Figures 8(a,b) and 10(a,b), it can be noted

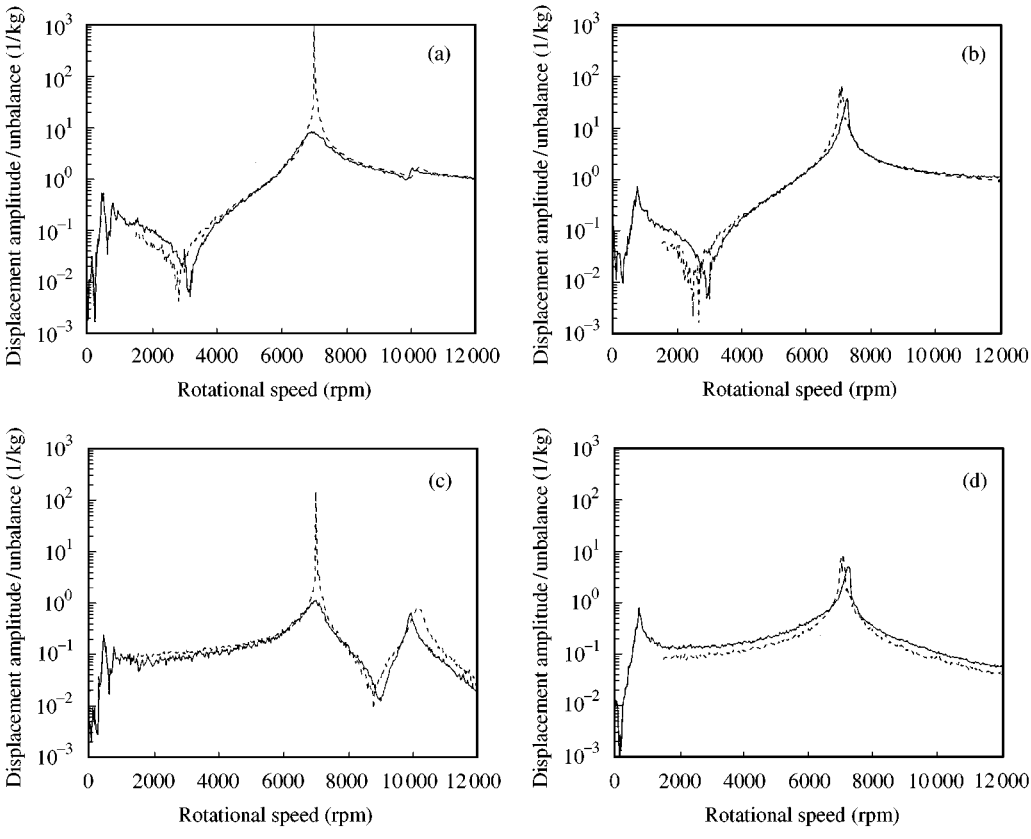

Figure 9. Absolute unbalance response in x and y directions at point P_3 and bearing pedestal No. 2 ($BP2$): predictions from *hybrid* model compared with measurement (hammer test). (a) Unbalance response at P_3 in x direction, (b) Unbalance response at P_3 in y direction, (c) Unbalance response at $BP2$ in x direction, (d) Unbalance response at $BP2$ in y direction. —— hammer test; – – – – hybrid model.

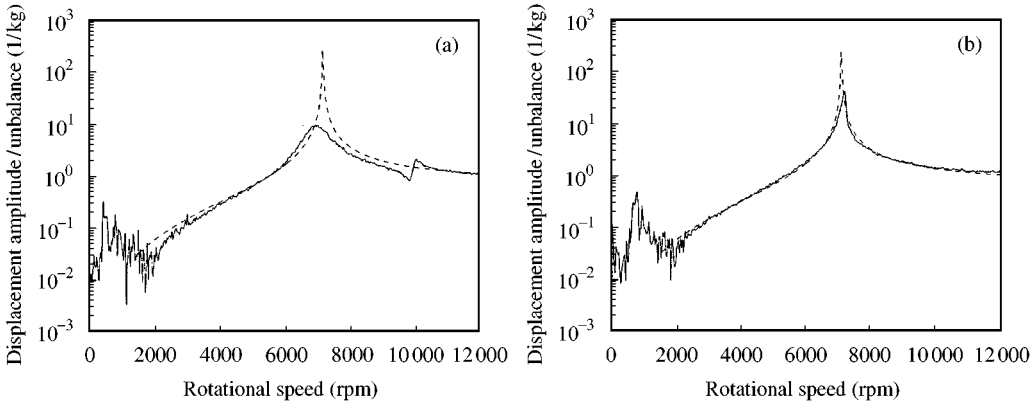

Figure 10. Relative unbalance response in x and y directions at point P_3: predictions from theoretical model compared with measurement (hammer test). (a) Unbalance response in x direction, (b) Unbalance response in y direction. ——, hammer test; – – – – theoretical model

that the antiresonance at around 2849 rpm in the absolute response (Figures 8a,b) does not appear in the relative response (Figures 10(a,b)). From Figures 10(a,b) it is also seen that for both simulation and measurement the relative responses in the x and y directions are

practically equal in magnitude at all speeds. They were also found to be in quadrature at all speeds which means that the shaft orbits should be *circular*, subject to the condition that the ball bearings remain linear in rotation. Because the relative responses in the x and y directions for both simulation and measurement are practically in quadrature at all speeds this indicates a low degree of damping despite relatively high damping in the bearings. This is attributed to the fact that the only damping forces in the system act at the bearings where the vibration of the shaft relative to the foundation (and hence the energy dissipation) is very low. The peak measured at around 13 Hz visible in all Figures 8–10 is the foam isolation resonance.

In Figures 11(a,b) the amplitudes of vibration in the x and y directions at point P_3, measured from the proximity probes are plotted for 18 speeds in the range 1500–6000 rpm. The theoretical response, obtained by multiplying the relative response in Figures 10a,b (which refers to an unbalance of 1 kg) by the added unbalance of 2×10^{-3} kg $\times 30 \times 10^{-3}$ m, is overlaid on the same axes. It is observed that the measured response is invariably greater than that predicted, which suggests that there is a high degree of unknown residual unbalance. It is also observed that for speeds greater than around 4250 rpm the slope of an imaginary curve through the measurement points roughly follows the slope of the theoretical curve, which indicates that indicates that the model is valid for these speeds. For speeds less than around 4250 rpm the slope of the curve through these points does not follow the slope of the theoretical curve. In fact, the measured orbits show that a transition from non-linearity to linearity occurs as the speed increases from 3500 to 4500 rpm and that this transition is characterized by a stage of chaos at 4000 rpm as shown in Figure 12(a). Such chaotic behaviour of ball bearings in rotation is described in reference [16]. For speeds above 4500 rpm the non-linearities disappear and the measured orbits are nearly perfect circles, as predicted (see Figure 12(b)).

Figures 13(a,b) compare the predictions for the absolute unbalance response at point P_3 with and without foundation movement taken into account: the inclusion of the foundation movement results in an *increase* in the first critical speed by 6%. This can be easily explained by considering a Jeffcott rotor of mass m supported on a floating rigid foundation of mass M. The fundamental resonance, $\omega_c = \sqrt{k(1+\mu)/m}$ (rad/s) where $\mu = m/M$ and k is the equivalent stiffness of the shaft and the bearings. Hence, since $\mu \neq 0$, ω_c is always greater than the fundamental resonance of the Jeffcott Rotor when mounted on a fixed foundation, $\omega_n = \sqrt{k/m}$.

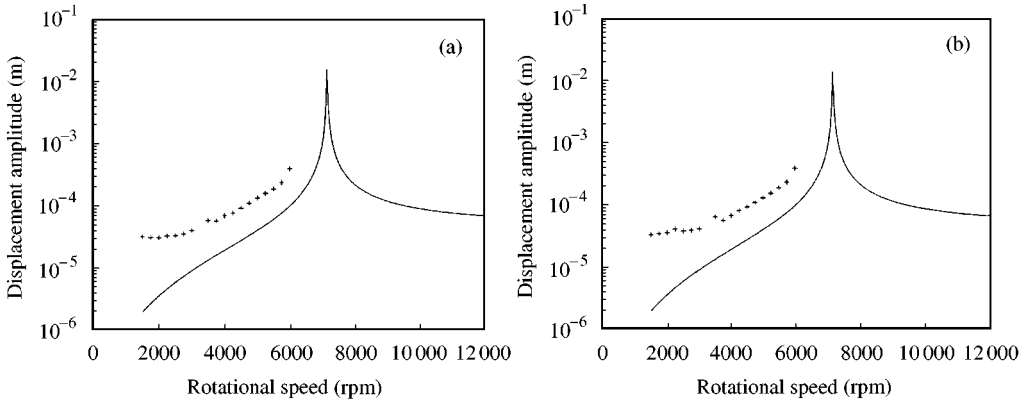

Figure 11. Relative unbalance response in x and y directions at point P_5: predictions from theoretical model compared with measurement (proximitors). (a) Unbalance response in x direction, (b) Unbalance response in y direction.——, theoretical model; + , measurement.

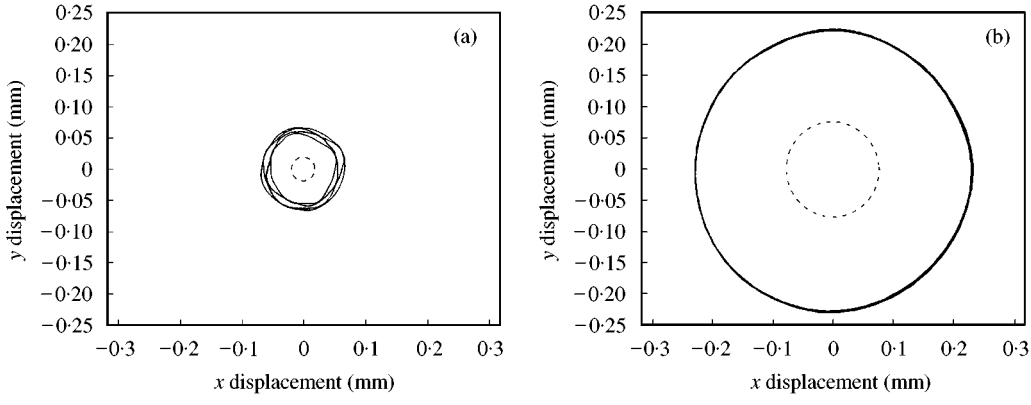

Figure 12. Orbits for rotational speeds 4000 and 5750 rpm (measured orbits: solid line, predicted orbits: dashed line). (a) 4000 rpm, (b) 5750 rpm.

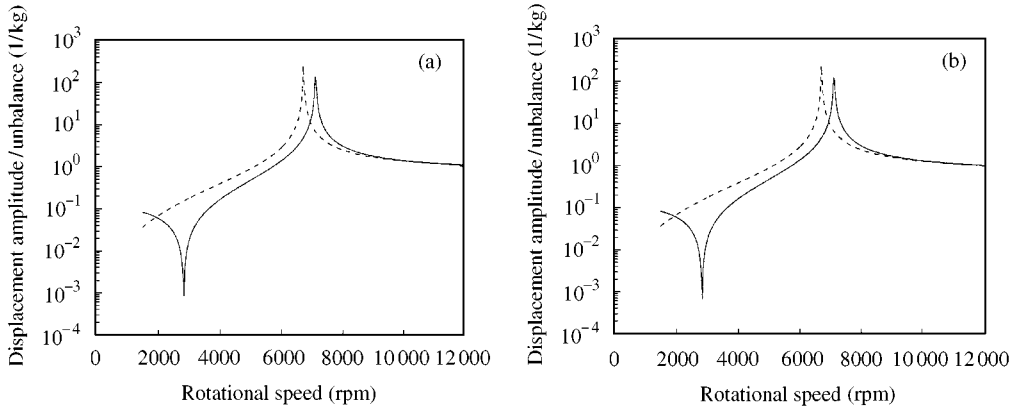

Figure 13. Comparison of predicted unbalance responses at point P_3 with and without foundation movement taken into account (theoretical model). (a) Unbalance response in x direction, (b) Unbalance response in y direction.—— moving foundation; – – – fixed foundation.

5. CONCLUSIONS AND FUTURE DEVELOPMENT

A mechanical impedance model of a coupled rotor-bearing-foundation system has been developed and partially validated in this paper. This modelling approach has the advantage that it can accomodate a mixture of theoretical and experimental models in the description of a coupled system. Two versions of the model were illustrated; an entirely theoretical model where the foundation was modelled as a beam and a hybrid model that included some measurements of the foundation dynamics. An error in the theoretical model prediction because of neglect of the torsional motion of the foundation was overcome by using the hybrid model. Gyroscopic effects were negligible in the test rig used and hence for the study reported here stationary testing using an impact hammer verified all aspects of the model developed except the assumption of linear behaviour of the ball bearings under rotating conditions. The measured shapes of the orbits showed that at low speeds non-linearities were evident in the test rig. However, these non-linearities disappeared at high speeds and circular orbits, as predicted by the model, were measured.

The main advantages of such a method are found to be the reduced number of degrees of freedom and the facility of including in the model either foundation dynamics

measurements, where this is possible, or an analytical model of the foundation. The latter need not be determined by the mechanical impedance method itself. The analogous dynamic stiffness method has been already been shown to be capable of determining natural frequencies and instability threshold speeds for rotor-bearing systems with linearized fluid film-bearing models. Moreover, although the mechanical impedance and its dynamic stiffness analogue ostensibly apply to linear systems, they can be applied to problems where linear elements are coupled with non-linear elements, for example a rotor supported on squeeze film bearings. The frequency response functions (mobilities, receptances) easily and directly computed with such methods for the linear subsystem can be included in harmonic balance calculations for the combined non-linear system. This is currently the subject of further research and will be reported on in the near future.

REFERENCES

1. H. D. NELSON 1998 *JSME International Journal Series C* **41**, 1–11. Rotordynamic modelling and analysis procedures: a review.
2. Z. WANG and J. W. LUND 1984 *Proceedings of the 3rd International Conference on Vibrations in Rotating Machinery*, *IMechE Conf. Publications*, 1984-10. *Vol.* C291/84, 13–15. Calculations of long rotors with many bearings on flexible foundations.
3. N. FENG, E. J. HAHN, A. LATTAB and A. SESTIERI 1992 *Vibrations in Rotating Machinery*, *IMechE* 1992-6, Vol. C432/142, 529–534. A combined finite element/transfer matrix approach for including foundation effects on the vibrating behaviour of rotating machinery.
4. S. RUBIN 1967 *The Journal of the Acoustical Society of America* **41**, 1171–1179. Mechanical Imittance and transmission matrix concepts.
5. V. H. NEUBERT 1987 *Mechanical Impedance*: *Modelling/Analysis of Structures*. Naval sea systems command, Code NSEA-55N.
6. R. G. KIRK, K. V. S. RAJU and K. RAMESH 1999 *The Shock and Vibration Digest* **31**, 449–454. PC-based analysis of turbomachinery vibrations.
7. N. F. REIGER, C. B. THOMAS and W. W. WALTER 1976 *Vibrations in Rotating Machinery*, *IMechE Conference Publications* 1976-9, Vol. C187/76, 187–193. Dynamic stiffness matrix approach for rotor-bearing analysis.
8. F. A. RAFFA, F. VATTA 1996 *Transactions of the ASME* **118**, 332–339. Dynamic stiffness methods for linear rotor-bearing systems.
9. E. KRAMER 1980 *Vibrations in Rotating Machinery*, *IMechE Conference Publications* 1980-4, Vol. C300/80, 333–338. Computation of the coupled rotor-machine foundation.
10. N. F. REIGER, S. ZHOU 1998 *Transactions of the ASME*, *Journal of Vibration and Acoustics* **120**, 240–251. Development and verification of transfer matrix unbalance response procedure for three-level rotor-foundation systems.
11. E. KRAMER 1993 *Dynamics of Rotors and Foundations*. Berlin: Springer.
12. R. H. LYON 1990 *Machinery Noise and Diagnostics*. London: Butterworths.
13. F. M. DIMENTBERG 1961 *Flexural Vibrations of Rotating Shafts*. London: Butterworths.
14. P. BONELLO 1998 M.Sc. Thesis, University of Southampton. Predicting the vibration response of a multi-span coupled rotor-bearing-foundation system by the mechanical impedance technique.
15. S. TIMOSHENKO, D. H. YOUNG, W. WEAVER Jr. 1974 *Vibration Problems in Engineering*. New York: Wiley, fourth edition.
16. H. TAMURA, E. H. GAD, A. SUEOKA 1986 *IFToMM Conference*: *Rotordynamics*, *Tokyo*, 553–560. Computer study of radial vibrations in a rotor/ball bearing system.

APPENDIX A: NOMENCLATURE

A	cross-sectional area of shaft/beam segment
E	Young's modulus
F_{fp} F'_{fp}	complex amplitudes of force at bearing pedestal no. p in x, y directions respectively
G	shear modulus

i	rotor station number ($i = 1, \ldots, M$)
I	second moment of area of shaft element section
I_p, I_t	polar and transverse moments inertia per unit length
I_{Pi}, I_{Ti}	polar and transverse moments of inertia of disc at rotor station no. i respectively
I_x, I_y	second moments of area of foundation section about neutral axis of bending in yz and xz planes respectively
$\bar{k}_{bxi}$	complex stiffness in x direction of bearing at rotor station no. i: $\bar{k}_{bxi} = k_{bxi}(1 + \mathrm{j}\eta_{bxi})$ where k_{bxi} is the elastic stiffness and η_{bxi} the loss factor; similarly for $\bar{k}_{byi}$, with respect to the y direction
$\bar{k}_{fxr}$	complex stiffness in x direction of foundation isolation mounting at foundation station no. r; $\bar{k}_{fxr} = k_{fxr}(1 + \mathrm{j}\eta_{fxr})$, where k_{fxr} is the elastic stiffness and η_{fxr} the loss factor; similarly for $\bar{k}_{fyr}$, with respect to the y direction
L	length of shaft/beam segment
m	mass per unit length
m_i	mass of disc at rotor station no. i
M_x, M_y	bending moments in xz and yz planes, respectively, at a general position z
M_{1n}, M'_{1n}	complex amplitudes of bending moment at left-hand (LH) end of shaft segment n in xz, yz planes respectively
M_{2n}, M'_{2n}	complex amplitudes of bending moment at right-hand (RH) end of shaft segment n in xz, yz planes respectively
n	shaft segment number ($n = 1, \ldots, M - 1$)
p	bearing pedestal number ($p = 1, \ldots, N$)
Q_x, Q_y	shear force in x and y directions, respectively, at a general position z
Q_{1n}, Q'_{1n}	complex amplitudes of shear force at LH end of shaft segment n in x, y directions respectively
Q_{2n}, Q'_{2n}	complex amplitudes of shear force at RH end of shaft segment n in x, y directions respectively
r	foundation station number ($r = 1, \ldots, R$)
r_0	radius of gyration about a diameter, $I_t = mr_0^2$
T (superscript)	transpose
V_{fp}, V'_{fp}	complex amplitudes of linear velocity of foundation in x, y directions, respectively, at bearing pedestal no. p
V_i, V'_i	complex amplitudes of linear velocity at rotor station no. i in x, y directions respectively
V_{1n}, V'_{1n}	complex amplitudes of linear velocity at LH end of shaft segment n in x, y directions respectively
V_{2n}, V'_{2n}	complex amplitudes of linear velocity at RH end of shaft segment n in x, y directions respectively
x, y	linear deflections at a general position z at time t in x and y directions respectively
X_i, Y_i	complex amplitudes of linear displacement at rotor station no. i in x, y directions respectively
ω	circular frequency of vibration (rad/s)
Ω	rotational speed of rotor (rad/s)
α	shear coefficient
ρ	material density
θ_x, θ_y	rotation of cross-section at a general position z at time t in xz and yz planes respectively
θ_i, θ'_i	complex amplitudes of angular deflections at rotor station no. i in xz, yz planes respectively
Ω_{1n}, Ω'_{1n}	complex amplitudes of angular velocities at LH end of shaft segment n in xz, yz planes respectively
Ω_{2n}, Ω'_{2n}	complex amplitudes of angular velocities at RH end of shaft segment n in xz, yz planes respectively